Thermodynamic and Kinetic Properties of Shocks in Two-Dimensional Yukawa Systems

M. Marciante and M. S. Murillo

Phys. Rev. Lett. **118**, 025001 — Published 10 January 2017

DOI: 10.1103/PhysRevLett.118.025001

Thermodynamic and kinetic properties of shocks in 2D Yukawa systems

M. Marciante[1] and M. S. Murillo[2,*]

[1] *Computational Physics and Methods Group, Los Alamos National Laboratory, Los Alamos, New Mexico 87544*[†]
[2] *Department of Computational Mathematics, Science and Engineering, Michigan State University, East Lansing, Michigan 48824*

Particle-level simulations of shocked plasmas are carried out to examine kinetic properties not captured by hydrodynamic models. In particular, molecular dynamics simulations of 2D Yukawa plasmas with variable couplings and screening lengths are used to examine shock features unique to plasmas, including the presence of dispersive shock structures for weak shocks. A phase-space analysis reveals several kinetic properties, including anisotropic velocity distributions, non-Maxwellian tails and the presence of fast particles ahead of the shock, even for moderately low Mach numbers. We also examine the thermodynamics (Rankine-Hugoniot relations) of recent experiments (Phys. Rev. Lett. **111**, 015002 (2013)) and find no anomalies in their equations of state.

Many limitations of hydrodynamic models of shock waves have been discovered using molecular dynamics (MD) simulations of hard-sphere gases [1, 2] and soft-potential molecular liquids [3–10]. Such a detailed understanding of shock waves is critical for a wide range of applications, including measurements of equations of state (EOS) [11, 12], medical therapies [13–15], traffic flows [16], high explosives [17], granular flows [18], particle acceleration [19–21], and astrophysical phenomena (supernovae [22], cosmic rays [23, 24], and solar wind [25]). In some fusion-energy devices [26–29], shock waves are used to compress a fuel to thermonuclear-burn conditions but are subject to detrimental hydrodynamic and kinetic instabilities. Recently, experiments employing video capture of shocked micron-scale charged particles [30] revealed shocks at the particle level [31–34] and, intriguingly, ideal-gas behavior in a very strongly coupled system.

We report the results of MD simulations of shock waves in 2D Yukawa systems, extending previous MD studies of shocks to plasma physics. We examined the EOS and kinetic properties by varying the plasma parameters (coupling and screening) and including Brownian dynamics relevant to recent experiments. By directly comparing the pre-shock and post-shock conditions, we validated the applicability of the Rankine-Hugoniot (RH) relations to 2D Yukawa systems with and without a damping mechanism, and we find agreement between theory and simulation. The role of damping in the shock region is also discussed; simulations revealed large deviations in shock structure due to damping, with important implications for dusty-plasma experiments. We varied the range of the interaction by varying the screening parameter to examine its impact on the Hugoniot EOS, and we find the perhaps-counterintuitive result that stronger screening leads to larger deviations from ideal-gas behavior. We also varied the interaction range and the shock strength to identify a region in parameter space for which a dispersive shock-wave (DSW) structure appears. Through visualizations of shocks in phase space, we examined a number of kinetic phenomena, including anisotropic and long-tail velocity distributions.

MD simulations were performed with identical particles of mass m interacting through the Yukawa potential

$$\beta U(r) = \Gamma e^{-\kappa r}/r, \tag{1}$$

where $\beta = (k_{\rm B}T)^{-1}$, Γ is the coupling parameter, $\kappa = a_i/\lambda_Y$ is the screening parameter, the 2D-ion sphere radius is a_i, the screening length is λ_Y, T is the temperature, $k_{\rm B}$ is the Boltzmann constant, and r is expressed in a_i units. We refer to the pre-shock and post-shock thermodynamic states with subscripts of 0 and 1, respectively. Initial plasma states (Γ_0, κ_0) were equilibrated via a Langevin thermostat, and they are characterized by their density $n_0 \equiv V_0^{-1}$, pressure p_0, temperature T_0 and sound speed $c_{s0} = \sqrt{(1+\Gamma_0/\kappa_0)/\beta_0 m}$ [35]. A moving, reflecting boundary condition modeled a piston moving at constant speed v_p in the z direction (piston Mach number $M_p = v_p/c_{s0}$). No data was recorded until a steady, planar shock with speed v_s had formed. Periodic boundary conditions were applied along the transverse direction (x axis). The parameters λ_Y and v_p were constant during the simulation, and a timestep $dt < 10^{-3}a_{i0}/v_p$ was found to acceptably suppress energy jumps caused by hard collisions at the shock front. Local measurements were made by dividing the simulation box into sub-cells over which thermodynamic quantities, including density, temperature and pressure, are computed [36]. A wide variety of initial states were chosen by independently varying the parameters Γ_0 and κ_0. First, we fixed $\kappa_0 = 1$, for which thermodynamic properties have been studied [37, 38] and the melting transition $\Gamma_c = 187$ is known, and varied the coupling parameter $\tilde{\Gamma}_0 = \Gamma_0/\Gamma_c$ from 10^{-3} to 5. To vary the range of the potential, we then fixed the coupling parameter $\Gamma_0 = 1517$ and varied the screening parameter $\kappa_0 \in \{0.28, 0.5, 1, 2, 5\}$. This value of Γ_0, together with $\kappa_0 = 0.28$, was chosen to correspond to the experimental conditions in [30].

Motivated by recent experiments [30], we searched for discrepancies with EOS relations for the 2D Yukawa system. In particular, we computed the post-shock pressure p_1 from the RH relations [39], given the initial state

$\{n_0, p_0\}$, the measured final density n_1 and the parameter v_p. This prediction was compared with direct local measurements of p_1 from the MD results; a perfect agreement was found. This confirmation is expected because the RH relations are simply a statement of conservation laws independent of interaction potentials and dimensionality; this finding confirms the validity of the experimental technique and of the non-equilibrium MD techniques, as well.

Measurements of the thermodynamic variables n and p yield the Hugoniots, which are parametrized by $p_1/p_0 = [1 - C\,(V_1/V_0)]\,[(V_1/V_0) - C]^{-1}$, where $C = \Delta h/\Delta e$ is the ratio of the jump in specific enthalpy h across the shock to the jump in specific internal energy e across the shock [39]. For a monoatomic ideal gas, $C = \gamma_d$, where $\gamma_d = 1+2/d$ is the adiabatic index in dimension d. Using the virial expression of the excess pressure $p_{ex} = \langle \mathbf{F} \cdot \mathbf{r} \rangle / Vd$, where the brackets stand for a statistical ensemble average, the following expression for C is obtained for the Yukawa potential:

$$C = \gamma_d + \frac{1}{d}\left(\kappa \frac{\Delta\langle rU\rangle}{\Delta e} - \frac{\Delta\langle U\rangle}{\Delta e}\right), \qquad (2)$$

where $\Delta\langle ...\rangle = \langle ...\rangle_1 - \langle ...\rangle_0$. Eqn. (2) cannot be evaluated further without solving the ensemble averages using MD, Monte Carlo or hypernetted-chain methods, but it shows that the value γ_d is only obtained as a coincidental cancellation or when the potential-energy jump is negligible compared to the kinetic-energy jump [40]. To confirm this behavior, we performed two MD studies by fixing either κ_0 or Γ_0, while varying the other parameter.

The results of 60 separate simulations with fixed $\kappa_0 = 1$ are shown in Fig. 1a for 12 values of $\Gamma = \{1, 2, 5\} \times \{10^{-3}, 10^{-2}, 10^{-1}, 1\}$ and 6 piston Mach numbers $M_p = 0, 0.2, 0.5, 1, 2, 5$. Results for varying piston speeds, increasing from right to left, tend to form groups, as shown by the dashed oval corresponding to $M_p = 0.2$. Although all results for the different couplings are very close to those for a 2D ideal gas, a small deviation is observed. Pressure jumps tend to be greater as the initial state is more strongly coupled. As expected for high Mach numbers, the data points match the ideal-gas curve because the ratios of potential- to kinetic-energy jumps are negligible. Fig. 1b shows Hugoniots for different screening parameters. The case $\kappa_0 = 0.28$ corresponds to the plasma state described in [30], although dust-neutral collisions are not yet included at this stage; interestingly, the Hugoniot for this particular state is the closest to the 2D ideal-gas curve. As screening increases, the pressure is shifted to higher values of C ($\gamma_3 < \gamma_2$), consistent with Eqn. (2) as the screening length gets smaller. Hence, the finding that dusty plasmas display ideal-gas behavior through the Hugoniot curve [30] is not related to a dynamical process involving damping from background species or to any fundamental property of 2D Yukawa

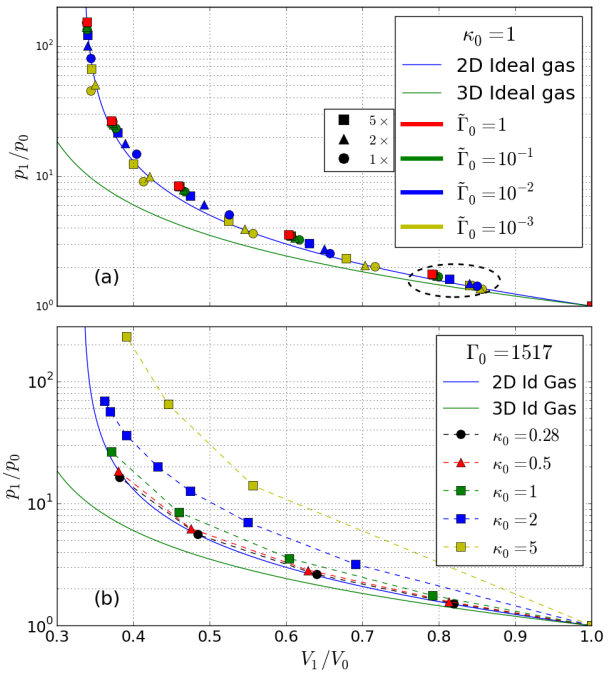

FIG. 1. Pressure ratio p_1/p_0 versus inverse compression V_1/V_0. (a) Fixed $\kappa_0 = 1$, with 12 values of Γ_0, and varying the shock strength (points in groups, as shown by dashed oval). The solid curves are the theoretical predictions for ideal gas behavior in 2D (blue) and 3D (green). This result shows that dimensionality plays a larger role than very large variations in coupling. (b) Same as (a), except for fixed $\Gamma_0 = 1517$. Hugoniots strongly deviate from the 2D-ideal gas curve as the screening is increased. Error bars, not shown, are smaller than the size of the markers.

systems, but appears to be a coincidental choice of parameters; the actual deviation from the ideal-gas curve can be very small compared with measurement errors. This prediction can be examined in future experiments.

The basic Yukawa model may not apply to certain experiments because of dissipative processes. In dusty plasmas, dust-neutral collisions cannot be neglected, in general, and they may impact the interpretation of shocked dusty plasmas. We examined the impact of such collisions on the stationary shock dynamics by including a drag force $\mathbf{F}_\eta = -\eta m \mathbf{v}$ [41]; essentially, the Langevin thermostat is employed *during* the simulation, albeit with different parameters known from experiments. For a drag coefficient $\eta/\omega_{p0} = 0.05$, where ω_{p0} is the plasma frequency of the initial state, the stationary shock dynamics shown in Fig. 2a and 2b are qualitatively different. For low piston Mach numbers M_p, the formation of a stationary shock is prevented by the drag force. For sufficiently high M_p, a shock is formed for which the downstream density profile linearly increases with the distance from the shock front, while the density jump remains the same as in the absence of damping. This result suggests that the RH relations, although derived from conserva-

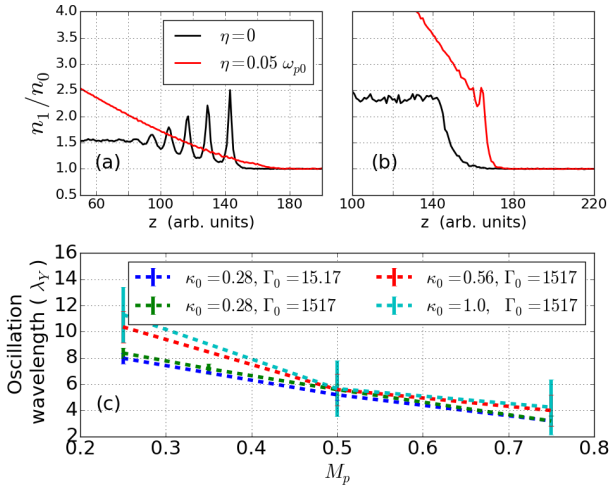

FIG. 2. (a,b) Effect of dust-neutral collisions on the shock dynamics. Density profiles are shown in the reference frame of the shock with (red) and without (black) damping for ($\Gamma = 1517, \kappa = 0.28$) and $M_p = 0.5$ (left panel (a)) and $M_p = 1.5$ (right panel (b)). Note the appearance of a strong DSW in the absence of damping in the weak shock case. In panel (c) we see how the wavelength of the first density oscillation varies as a function of the piston Mach number for several plasma states.

tion laws, remain locally valid across a shock front in the presence of low damping. The density profiles shown in Fig. 2 do not reflect those obtained in dusty plasma experiments, which have so far generated blast waves [30, 32]. In the supplemental material [45], we discuss the difference between steady shocks and blast waves, for which results of an appropriate model are shown.

The shock wave produced in the undamped plasma shown in Fig. 2a displays a very pronounced DSW, a phemonena observed experimentally in collisionless plasmas [42], and predicted in the very weak shock limit by means of a small-parameter expansion of the non-linear dynamics [43]. We quantify the influence of the plasma parameters on the DSW by measuring the distance between the two first peaks of the density oscillation with respect to the Mach number in Fig. 2c. The error estimate is large because of the finite size of the space discretization over which the density is computed. As the Mach number increases towards unity, the DSW exhibits shorter wavelengths and fewer oscillations, effectively vanishing for $M_p = 1$ (no DSW is seen in Fig. 2b for $M_p = 1.5$). That the density-oscillation length decreases as the screening parameter increases reflects the dominant role played by the particle collective modes induced by the long-range force field (plasma behavior). We also performed a series of simulations of 3D Yukawa systems (not shown) using coupling and screening parameters equivalent to those presented here and found very similar results.

While the RH relations connect the asymptotic thermodynamic states away from the shock front, they do not contain any dynamical information about the shock region itself. To study kinetic effects in this region, we average the MD data at a given ζ-position ($\zeta = z - v_s t$) to compute the 1-particle distribution function $f_1(\zeta, v_z)$ in the reference frame of the shock. Fig. 3 shows the resulting $f_1(\zeta, v_z)$ distribution functions for a plasma state ($\Gamma = 1517, \kappa = 0.5$) at three different piston Mach numbers $M_p = 0.5$ (3a), 0.8 (3b) and 1.0 (3c), corresponding to shock Mach numbers $M_s = 1.1$, 1.5 and 1.8, respectively. Through an analysis of the phase space distribution function f_1 we can assess the accuracy of hydrodynamic models, which are typically constructed from perturbations around a local Maxwell velocity distribution (Chapman-Enskog expansion). Here, we define "kinetic" to refer to any deviation from a local, spherical Maxwellian distribution [52].

To determine whether the DSW could be accurately reproduced using a hydrodynamic model, we use the kinetic information provided by MD to compute the local value of the work $w_z = \langle F_\zeta v_z \rangle$, with the force F_ζ acting on particles at position ζ inside the plasma DSW. For the case $M_p = 0.5$ shown in Fig. 3a, we found that the equality $\langle F_\zeta v_z \rangle = \langle F_\zeta \rangle \langle v_z \rangle$ holds and that it should allow for an accurate description of the DSW using a mean-field model of the shock. As the Mach number increases, this equality breaks down at the shock front; thus, small-scale correlations and collisional processes cannot be neglected in an analysis of the damping mechanism of the DSW.

Moments of f_1 also reveal kinetic effects; for example, a strong anisotropy is found to occur at the shock front, as seen in Fig. 3e and f. Here, the second moment of f_1 along the propagation of the shock (σ_z, red curves) and transverse to its propagation (σ_x, blue curves) are shown to exhibit very different behaviors indicative of anisotropic temperatures. At $M_p = 0.5$, these two velocity components exhibit similar oscillations despite the fact that the DSW modulates the density along only the z direction. Here, collisional processes are faster than the DSW dynamics and allow for efficient energy and momentum exchange between the two velocity components. At higher Mach numbers, however, the two moments exhibit a very different evolution: σ_x increases almost monotonically through the shock front (a small peak is visible near the peak density position); in contrast, σ_z increases through the shock front and reaches a peak value twice as high as its final equilibrium value at a position not corresponding to peak density. Holian and coworkers [44] have shown that, for a hard-sphere gas, a model beyond Navier-Stokes is necessary to provide an accurate hydrodynamic description of this behavior, which occurs in this plasma state ($\Gamma_0 = 1517, \kappa_0 = 0.5$) for a shock Mach number as low as $M_s = 1.5$. Note, however, that our results in Fig. 3b and c also show a fast-particle tail near the shock, as indicated by the white arrows.

We can further quantify these kinetic effects by considering higher-order central moments $\langle \Delta v_z^4 \rangle$ normalized by

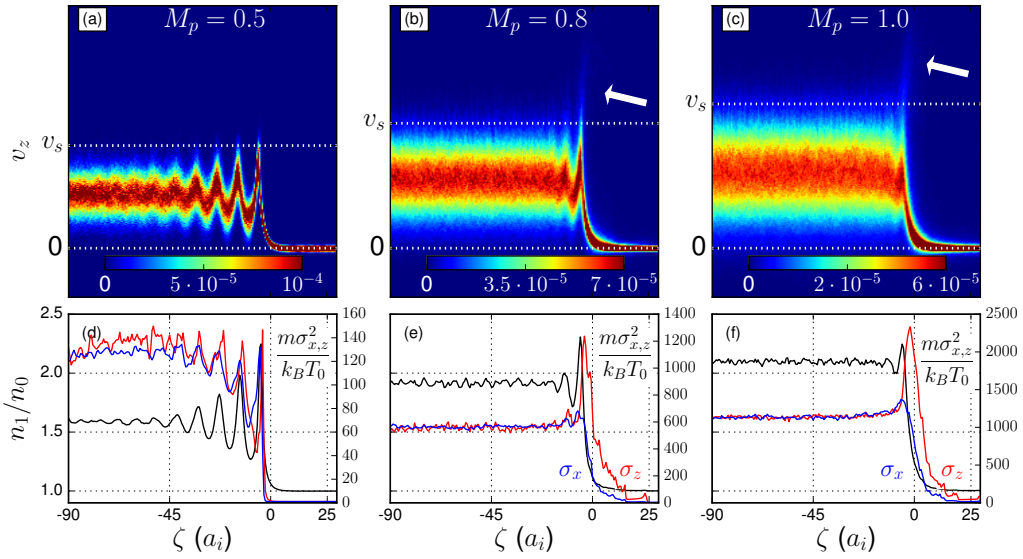

FIG. 3. Kinetic properties of plasmas in phase-space. The 1-particle distribution function $f_1(\zeta, v_z)$ is seen in the reference frame of the shock (velocities are shifted by $+v_s$) for plasma parameters $\Gamma_0 = 1517$ and $\kappa_0 = 0.5$, at piston Mach numbers (a) $M_p = 0.5$, (b) $M_p = 0.8$ and (c) $M_p = 1$. Figures (d), (e) and (f) show the corresponding density profiles (black curve - left axis) and normalized second moment σ_z (red curve - right axis) and σ_x (blue curve - right axis) of velocity distributions. Right arrows show the existence of a strong non-Maxwellian tail corresponding to velocities higher than the shock speed.

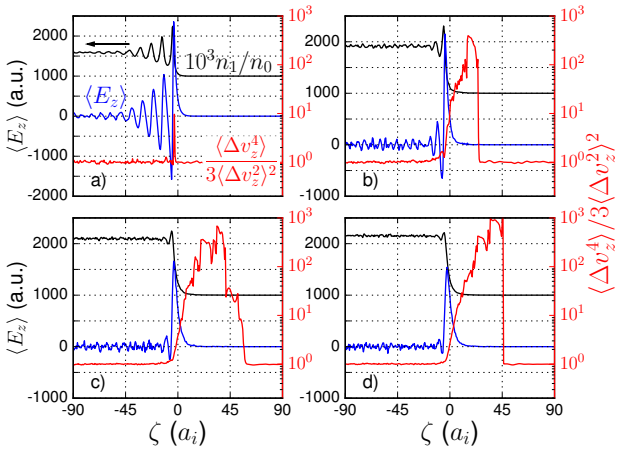

FIG. 4. Deviation from the Maxwell velocity distribution. Plots show the relative density profile (value increased by a factor 10^3, black curve - left axis), the z-component of the electric field $\langle E_z \rangle$ (blue curve - left axis) and the fourth central moment ($\Delta v = v - \langle v \rangle$) of the local v_z-velocity distribution $\langle \Delta v_z^4 \rangle$ divided by its theoretical Maxwellian value $3\langle \Delta v_z^2 \rangle^2$ (red curve - right axis) for $M_p = 0.5$ (a), 0.8 (b), 1 (c) and 2 (d), for plasma parameters $\Gamma = 1517$ and $\kappa = 0.5$.

the theoretical Maxwellian value $3\langle \Delta v_z^2 \rangle^2$, where $\Delta v = v - \langle v \rangle$; these are shown in Fig. 4 for $M_p = 0.5, 0.8, 1, 2$. This normalization is chosen to be unity in an equilibrium state. For the smallest Mach number, the ratio $\langle \Delta v_z^4 \rangle / 3\langle \Delta v_z^2 \rangle^2$ shows a narrow peak of value 10 at the position of the first density peak. For greater Mach numbers, the ratio reaches values greater than 10^2 ahead of the shock front over a distance of several tens of ion sphere radii a_{i0}. This finding shows that the viscous width of the shock front may not be the most relevant measure for quantifying the extent of the shock, but rather a "shock zone" that includes fast particles streaming ahead of the shock (and preheating material there). We surmise that these fast particles are created by the strong electric field at the shock front (blue curve in Fig. 4), which accelerates particles into the tail of the v_z-velocity distribution, likely generating a non-local transport of particles.

In summary, extensive non-equilibrium MD simulations of shocks in plasmas have been conducted. Distant from the shock front, we find excellent agreement with the RH relations, and we have obtained thermodynamics properties from the simulations. We do not find any anomalies with the EOS of shocked 2D Yukawa systems, even when background damping is included in the simulations. Rather, we find that recent experiments merely probe a regime of parameter space for which the Hugoniot of a strongly coupled system is similar to its ideal gas limit. Our results reveal non-Maxwellian behavior near the shock in the form of both anisotropic velocity distributions and the generation of fast particles moving ahead of the shock. These observations have implications for the modeling of shocks in terms of low-order hydrodynamic descriptions (e.g., Euler or Navier-Stokes) and for experiments in which preheating of unshocked material is important. We also observe shock structures with dispersive properties, a plasma property not seen in previous MD simulations of shocked hard-sphere or soft-potential

liquids. In general, these results highlight how atomic-scale MD simulations can be used to examine hydrodynamic properties of plasmas, and further MD studies of hydrodynamic phenomena, such as waves, instabilities, and laser-matter interactions, are warranted.

The authors thank Prof. J. Goree for fruitful discussions. This work has been performed under the NAMBE Project as part of Los Alamos National Laboratory Contract DE-AC52-06NA25396. This document is LA-UR-16-28297.

* https://murillogroupmsu.com; murillom@msu.edu
† mmarciante@lanl.gov

[1] E. Salomons and M. Mareschal, Phys. Rev. Lett. **69**, 269 (1992).
[2] F.J. Uribe, R.M. Velasco and L.S. Garcia-Colin, Phys. Rev. Lett. **81**, 2044 (1998).
[3] B.L. Holian and G.K. Straub, Phys. Rev. Lett. **43**, 1598 (1979).
[4] B.L. Holian, W.G. Hoover, B. Moran and G.K. Straub, Phys. Rev. A **22**, 2798 (1980).
[5] B.L. Holian, Phys. Rev. A **37**, 2562 (1988).
[6] V.V. Zhakhovskiĭ, S.V. Zybin, K. Nishihara and S.I. Anisimov, Phys. Rev. Lett. **83**, 1175 (1999).
[7] T.C. Germann, B.L. Holian, P.S. Lomdahl,and R. Ravelo, Phys. Rev. Lett. **84**, 5351 (2000).
[8] B.L. Holian, T.C. Germann, J.-B. Maillet and C.T. White, Phys. Rev. Lett. **89**, 285501 (2002).
[9] T. Hatano, Phys. Rev. Lett. **92**, 015503 (2004).
[10] H.Liu, W. Kang, Q. Zhang *et al.*, Front. Phys. **11**, 115206 (2016).
[11] J.H. Nguyen and N. Holmes, Nature **427**, 339 (2004).
[12] J. Zheng, Q. Cheng, G. Yunjun and Z. Shen, Sci. Rep. **5**, 16041 (2015).
[13] C.H. Chaussy, W. Brendel and E. Schmiedt, The Lancet **316**, 1265 (1980).
[14] M. Delius, G. Enders, Z. Xuan *et al.*, Ultrasound in Med. and Biol. **14**, 117 (1988).
[15] A. Nakagawa, G.T. Manley, A.D. Gean *et al.*, J. Neurotrauma. **28**, 1101 (2011).
[16] P.I. Richards, Operations Research **4**, 42 (1956).
[17] C.M. Tarver, S.K. Chidester and A.L. Nichols III, J. Phys. Chem. **100**, 5794 (1996).
[18] A. Vilquin, J.F. Boudet and H. Kellay, Phys. Rev. E **94**, 022905 (2016).
[19] L.O. Silva, M. Marti, J.R. Davies and R.A. Fonseca, Phys. Rev. Lett. **92**, 015002 (2004).
[20] M.S. Wei, S.P.D. Mangles, Z. Najmudin *et al.*, Phys. Rev. Lett. **93**, 155003 (2004).
[21] F. Fiuza, A. Stockem, E. Boella *et al.*, Phys. Rev. Lett. **109**, 215001 (2012).
[22] S. Campana, V. Mangano, A.J. Blustin *et al.*, Nature **442**, 1008 (2006).
[23] J. Bednarz and M. Ostrowski, Phys. Rev. Lett. **80**, 3911 (1998).
[24] F.A. Aharonian, A.G. Akhperjanian, K.-M. Aye *et al.*, Nature **432**, 75 (2004).
[25] R. Prangé, L. Pallier, K.C. Hansen *et al.*, Nature **432**, 78 (2004).
[26] V.N. Goncharov, O.V. Gotchev, E.Vianello *et al.*, Physics of Plasmas **13**, 012702 (2006).
[27] R. Betti, C.D. Zhou, K.S. Anderson *et al.*, Phys. Rev. Lett. **98**, 155001 (2007).
[28] L.J. Perkins, R. Betti, K.N. LaFortune and W.H. Williams, Phys. Rev. Lett. **103**, 045004 (2009).
[29] M. Temporal, B. Canaud, W.J. Garbett and R. Ramis, Physics of Plasmas **22**, 102709 (2015).
[30] N.P. Oxtoby, E.J. Griffith, C. Durniak *et al.*, Phys. Rev. Lett. **111**, 015002 (2013).
[31] F. Li and O. Havnes, Phys. Rev. E **64**, 066407 (2001).
[32] D. Samsonov, S.K. Zhdanov, R.A. Quinn *et al.*, Phys. Rev. Lett. **92**, 255004 (2004).
[33] J. Heinrich, S.-H. Kim and R.L. Merlino, Phys. Rev. Lett. **103**, 115002 (2009).
[34] Y. Saitou, Y. Nakamura, T. Kamimura and O. Ishihara, Phys. Rev. Lett. **108**, 065004 (2012).
[35] M.S. Murillo and D.O Gericke, J. Phys. A: Math. Gen. **36**, 6273 (2003).
[36] T.W. Lion and R.J. Allen, J. Phys.: Condens. Matter **24**, 284113 (2012).
[37] O.S. Vaulina, X.G. Koss, Physics Letters A **373**, 3330 (2009).
[38] T. Ott, M. Stanley and M. Bonitz, Phys. Of Plasmas **18**, 063701 (2011).
[39] Ya.B. Zel'dovich and Yu.P. Raizer, *Physics of Shockwaves and and High Temperature Hydrodynamic Phenomena* (Academic, New York, 1967).
[40] It is worth noting that a pair-interaction potential $U \propto r^{-2}$ would exactly satisfy the relation $C = \gamma_d$ and would result in an exact ideal-gas behavior.
[41] S.A. Khrapak, A.V. Ivlev, G.E. Morfill and H.M. Thomas, Phys. Rev. E **66**, 046414 (2002).
[42] R.J. Taylor, D.R. Baker and H. Ikezi, Phys. Rev. Lett. **24**, 206 (1970).
[43] H. Washimi and T. Taniuti, Phys. Rev. Lett. **17**, 996 (1966).
[44] B.L. Holian, C.W. Patterson, M.Mareschal and E. Salomons, Phys. Rev. E **47**, R24 (1993).
[45] See Supplemental Material [url], which includes Refs. [46–51].
[46] P.L. Sachdev, Shock waves & explosions, CRC Press (2004).
[47] M.D. Knudson, D.L. Hanson, J.E. Bailey, C.A. Hall and J.R. Asay, Phys. Rev. Lett. **87**, 225501 (2001).
[48] M.D. Knudson, D.L. Hanson, J.E. Bailey, C.A. Hall, J.R. Asay and C.Deeney, Phys. Rev. B **69**, 144209 (2004).
[49] D.G. Hicks, N.B. Meezan, E.L. Dewald *et al.*, Physics of Plasmas. **19**, 122702 (2012).
[50] G. Taylor, Proceedings of the Royal Society of London. Series A, Mathematical and Physical Sciences **201**, 159 (1950).
[51] D.F. Cioffi, C.F. Mckee and E. Bertschinger, The Astrophysical Journal **334**, 252 (1988).
[52] Strictly speaking, this definition corresponds to "beyond-Euler" hydrodynamics. For small deviations, the first-order Chapman-Enskog expansion includes transport processes at the Navier-Stokes level. An alternate definition of "kinetic," therefore, is "beyond Navier-Stokes," which is the Burnett level [1]. In general, the terms "kinetic" and "deviations from hydrodynamics" are poorly defined.